




Human influenza A virus causes myocardial and cardiac-specific conduction system infections associated with early inflammation and premature death

David Filgueiras-Rama ^{1,2,3‡}, Jasmina Vasilijevic^{4,5‡}, Jose Jalife^{2,3,6}, Sami F. Noujaim⁷, Jose M. Alfonso², Jose A. Nicolas-Avila², Celia Gutierrez⁴, Noelia Zamarreño⁴, Andres Hidalgo ², Alejandro Bernabé², Christopher Pablo Cop², Daniela Ponce-Balbuena ⁶, Guadalupe Guerrero-Serna ⁶, Daniel Calle ^{2,8}, Manuel Desco^{2,8,9,10}, Jesus Ruiz-Cabello ^{5,11,12,13}, Amelia Nieto^{4,5}, and Ana Falcon ^{4,5*†}

¹Cardiac Electrophysiology Unit, Hospital Clínico San Carlos, Madrid, Spain; ²Centro Nacional de Investigaciones Cardiovasculares (CNIC), Madrid, Spain; ³Consortium CIBER of Cardiovascular Diseases (CIBERCv), Spain; ⁴Department of Molecular and Cellular Biology, National Center for Biotechnology, Spanish National Research Council, Madrid, Spain; ⁵Consortium CIBER of Respiratory Diseases, Spain; ⁶Center for Arrhythmia Research, Health System, University of Michigan, MI, USA; ⁷Morsani College of Medicine Molecular Pharmacology & Physiology, University of South Florida, Tampa, FL, USA; ⁸Instituto de Investigación Sanitaria Gregorio Marañón, Madrid, Spain; ⁹Department of Bioengineering and Aerospace Engineering, University Carlos III of Madrid, Madrid, Spain; ¹⁰Consortium CIBER of Mental Health (CIBERSAM), Spain; ¹¹Center for Cooperative Research in Biomaterials (CIC biomaGUNE), Basque Research and Technology Alliance (BRTA), San Sebastian, Spain; ¹²IKERBASQUE, Basque Foundation for Science, Spain; and ¹³Universidad Complutense Madrid, Madrid, Spain

Received 21 January 2020; revised 27 March 2020; editorial decision 15 April 2020; accepted 22 April 2020; online publish-ahead-of-print 20 May 2020

Time for primary review: 20 days

Aims

Human influenza A virus (hIAV) infection is associated with important cardiovascular complications, although cardiac infection pathophysiology is poorly understood. We aimed to study the ability of hIAV of different pathogenicity to infect the mouse heart, and establish the relationship between the infective capacity and the associated *in vivo*, cellular and molecular alterations.

Methods and results

We evaluated lung and heart viral titres in mice infected with either one of several hIAV strains inoculated intranasally. 3D reconstructions of infected cardiac tissue were used to identify viral proteins inside mouse cardiomyocytes, Purkinje cells, and cardiac vessels. Viral replication was measured in mouse cultured cardiomyocytes. Human-induced pluripotent stem cell-derived cardiomyocytes (hiPSC-CMs) were used to confirm infection and study underlying molecular alterations associated with the *in vivo* electrophysiological phenotype. Pathogenic and attenuated hIAV strains infected and replicated in cardiomyocytes, Purkinje cells, and hiPSC-CMs. The infection was also present in cardiac endothelial cells. Remarkably, lung viral titres did not statistically correlate with viral titres in the mouse heart. The highly pathogenic human recombinant virus PAmut showed faster replication, higher level of inflammatory cytokines in cardiac tissue and higher viral titres in cardiac HL-1 mouse cells and hiPSC-CMs compared with PB2mut-attenuated virus. Correspondingly, cardiac conduction alterations were especially pronounced in PAmut-infected mice, associated with high mortality rates, compared with PB2mut-infected animals. Consistently, connexin43 and Na_v1.5 expression decreased acutely in hiPSC-CMs infected with PAmut virus. YEM1L protease also decreased more rapidly and to lower levels in PAmut-infected hiPSC-CMs compared with PB2mut-infected cells, consistent with mitochondrial dysfunction. Human IAV infection did not increase myocardial fibrosis at 4-day post-infection, although PAmut-infected mice showed an early increase in mRNAs expression of lysyl oxidase.

* Corresponding author. Tel: +34 686905842, E-mail: anafalcon.af@gmail.com

†Present address. Algenex S.L., Madrid, Spain.

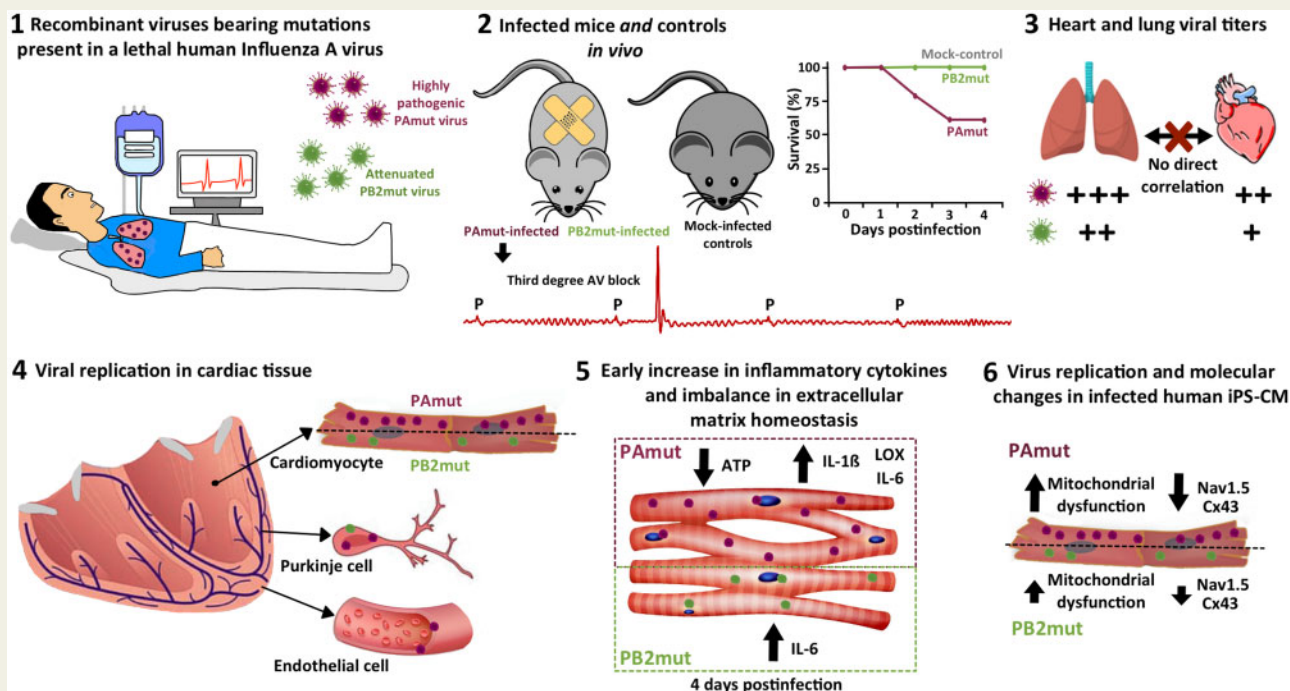
‡The first two authors contributed equally to the study.

© The Author(s) 2020. Published by Oxford University Press on behalf of the European Society of Cardiology.

This is an Open Access article distributed under the terms of the Creative Commons Attribution Non-Commercial License (<http://creativecommons.org/licenses/by-nc/4.0/>), which permits non-commercial re-use, distribution, and reproduction in any medium, provided the original work is properly cited. For commercial re-use, please contact journals.permissions@oup.com

Conclusion

Human IAV can infect the heart and cardiac-specific conduction system, which may contribute to cardiac complications and premature death.

**Keywords**

Human influenza A virus • Heart infection • Viral replication • Premature death

1. Introduction

The influenza A virus (IAV) is a major contributor to acute respiratory infections,¹ but its pathogenicity is not limited to respiratory damage. Various complications in non-respiratory tissues (e.g. encephalopathy) have been described during seasonal influenza infections.^{2,3} Among others, myocarditis and congestive heart failure have been associated with IAV infection.⁴⁻⁹ Focal-to-diffuse myocarditis has been reported during the Asian and 1918 influenza pandemics.¹⁰ More recently, during the 2009 pandemic, cardiac complications have been described in 4.9% of hospitalized patients, and up to 46% of patients admitted to intensive care units.¹¹ Current evidence also indicates that, in patients with pre-existing atherosclerotic disease, pulmonary infection induces an inflammatory response that may trigger an acute coronary syndrome.¹² Moreover, severe ventricular arrhythmia with fatal consequences and high-degree atrio-ventricular block have been also reported in infected patients, even without apparent respiratory damage.^{13,14}

Despite potential IAV-related cardiac damage after infection, the rare reports showing viral material in the human myocardium remain unconfirmed.¹⁵ Moreover, human IAV pathophysiology in cardiac tissue and the associated *in vivo*, cellular and molecular alterations remain unexplored. Thus, current understanding mostly assumes that cardiac

pathology on human IAV infection is directly related to respiratory tract damage and a subsequent inflammatory reaction that may lead to cardiac complications in patients with significant comorbidities.^{12,16}

Importantly, during the process of identifying the pathogenicity factor of a lethal influenza A virus (F-IAV) isolated from the 2009 pandemic,¹⁷ we generated recombinant viruses carrying mutations in PA and PB2 viral polymerase subunits of F-IAV on the A/H1N1/California/04/09 virus backbone (CAL).¹⁷ The use of a recombinant virus carrying PA D529N (PAmut) showed that this mutation was responsible for the augmented pathogenicity of the F-IAV isolate, while a recombinant virus with the mutation PB2 A221T (PB2mut) was attenuated in mice.¹⁷ Here, we hypothesize that human IAV can also infect and replicate in the mouse heart and cultured cardiomyocytes. Moreover, cardiac damage and underlying molecular alterations will be directly associated with virus pathogenicity, although cardiac infection and viral titres in heart tissue will not necessarily follow a direct relationship with lung titres. We tested this hypothesis using pathogenic PAmut and attenuated PB2mut recombinant viruses to explore the ability of human IAV to infect and trigger cardiac damage in infected mice *in vivo*, heart tissue samples and cultured cardiomyocytes. We also studied the underlying molecular alterations associated with the *in vivo* virus-related electrophysiological phenotype using infected human-induced pluripotent stem cell-derived

cardiomyocytes (hiPSC-CMs). Altogether, our data report direct cardiac infection and heart damage related to human IAV pathogenicity and not necessarily related to lung viral titres, which may contribute to the severity or even fatality of influenza virus infections in humans.

2. Methods

The *in vivo* studies were conducted in accordance with institutional guidelines and National, European, and US National Institute of Health guidelines for the care and use of laboratory animals. Protocols were approved by the National Center for Biotechnology Ethics Committee on Animal Experimentation (permit no. 11014) and Institutional Animal Care and Use Committee of the University of Michigan (approval no. PRO0006827). Animals were anesthetized with isoflurane (3%) in an inhalation chamber before viral inoculation. Animals were euthanized with isoflurane (7%) inhalation followed by a second euthanasia method (bilateral pneumothorax or removal of vital organs, lungs and/or heart as indicated). *Figure 1* shows a flow-chart with all the experimental sets.

2.1 Biological materials

Cell lines used in this study were MDCK (canine kidney; ATCC CCL-34), and cardiac HL-1 (mouse). Human-induced PSC-CMs were derived from iCell™ cardiomyocytes obtained from Cellular Dynamics International (Madison, WI) using a modified protocol previously described elsewhere¹⁸ (more details in [Supplementary material online](#)). Briefly, the iCell™ cardiomyocytes were thawed and plated in differentiation medium (EB20), and 24 h later, medium was switched to RPMI plus B27 supplement with insulin (Gibco). Antibodies to GAPDH, β -actin (both from Sigma), and rabbit anti-NP-PB1 antibodies were used for western blot.^{19,20} Western-blot assays were performed as described elsewhere.²¹

2.2 Cell infection

Cultured mouse HL-1 cells were infected at 10^{-3} or 3–5 plaque-forming units (pfu)/cell as indicated in each experiment. Cells were used for western-blot and immunofluorescence analyses, and supernatants were used for virus titration by standard plaque assay.²² Human iPSC-CM cultures were Mock-infected or infected with PAmut or PB2mut recombinants at 3 multiplicity of infection (moi).

2.3 Mice with Connexin40 and green-fluorescent protein (Cx40^{eGFP})

We used Cx40^{eGFP} mice to enable visualization of the Purkinje network via GFP expression. Founders for our Cx40^{eGFP} mouse colony were generously provided by the laboratory of Dr Daniel Gros at Université de la Méditerranée, Marseille, France. Generation and characterization of these transgenic mice have been described in detail previously.²³ Briefly, these mice were generated by insertion of the eGFP coding sequence into the *GJA5* gene locus by homologous recombination, and were maintained under a mixed genetic background (CD1/129 Sv). Heterozygous offspring were intercrossed to obtain homozygously mutated progeny, as described elsewhere.²³

2.4 *In vivo* virus infections in mice

All animal studies were performed under biosafety level 2+ conditions. Female BALB/c ANNHsd mice (6 weeks old) were infected intranasally with the corresponding recombinant viruses at 10^6 or 10^3 plaque-

forming units (pfu) as indicated in each experiment or were Mock-infected. Female Cx40^{eGFP} mice (7 weeks old) were also infected intranasally with PAmut or PB2mut viruses at 10^6 pfu, or were Mock-infected. All animals were monitored daily for body weight. For ethical reasons, in all experiments, mice were euthanized when a 25% body weight loss was documented. Total heart or lung extracts were used for viral titre determination by plaque assay, biochemical analysis, or confocal immunofluorescence as described below.

2.5 Immunostaining and confocal microscopy of cardiac tissue and cultured cells

Mock, PAmut-, and PB2mut-infected HL-1 cells were collected at specified hours post-infection (hpi), fixed with methanol for 20 min at -20°C and stored in phosphate-buffered saline. Cells were incubated with a primary rabbit anti-NP antibody¹⁹ and subsequently incubated with a secondary Alexa 594-conjugated goat anti-rabbit antibody (Molecular Probes, Eugene, Oregon).

Mock, PAmut-, and PB2mut-infected mouse hearts were collected, fixed in 15% formalin, and embedded in paraffin [for wild-type (WT) hearts] or optimum cutting temperature compound (for Cx40^{eGFP} hearts). About 8- to 10 μm slices were obtained using a microtome. Prior to use, paraffin samples were deparaffinized and hydrated. Epitope unmasking was performed using DAKO target retrieval solution (Ref. S1699) in a PTlink equipment (DAKO). The samples were used for confocal microscopy using DAPI, and the following primary antibodies: rabbit anti-NP, rat anti-NP,²⁴ and rabbit anti-laminin (polyclonal; Sigma); and secondary antibodies: chicken anti-rat AF647 and goat anti-rabbit AF488/AF546 (Molecular Probes, Eugene, Oregon). All images were obtained using an SPE confocal microscope (Leica). The NP+ area was calculated using a threshold based on absolute intensity and automatic quantification with Fiji (National Institutes of Health, USA).

2.6 Histopathology analysis

Ventricular cross-sections from both WT and Cx40^{eGFP} mice were dehydrated and cut into 10- μm thick sections. Haematoxylin and eosin (H&E) stained sections were digitized using a NanoZoomer S360 Digital slide scanner (Hamamatsu, Japan) for subsequent analysis. Sequential analysis of stained samples was performed to identify any regions with overt conventional histopathologic features of coagulative necrosis, including elongated and pyknotic nuclei, loss of the striated cardiomyocyte structure, slight increases in colour intensity, and glassy cytoplasm.²⁵

Tissue slices were also stained with Masson Trichrome and digitized using a NanoZoomer S360 Digital slide scanner (Hamamatsu, Japan) for analysis. A total of five randomly selected $20\times$ insets per slide were analysed. Interstitial fibrosis was quantified using ImageJ. Colour threshold hue (scale: 0–255) was adjusted for each image to include only blue pixels (scale: 115–210), corresponding to collagen fibres, and the values for each area were recorded. Fibrosis proportion (blue staining areas/total tissue area) was measured in every inset and a mean value was assigned to each sample.

2.7 ATP quantification

ATP content was assessed by ATP Bioluminescence Assay Kit CLS II (Roche, Mannheim, Germany) according to the manufacturer's instructions.

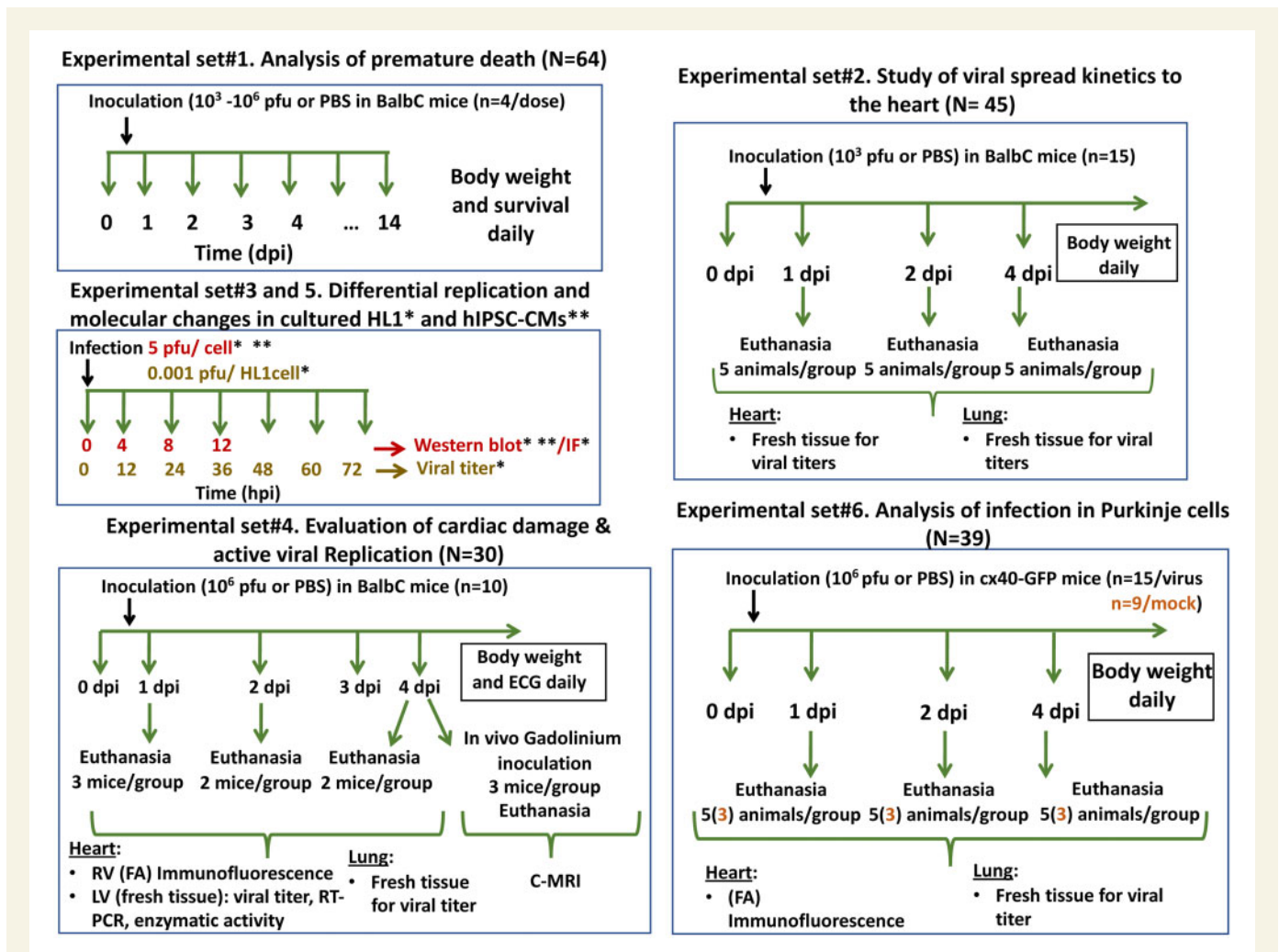


Figure 1 Flowchart showing all the experimental sets. C-MRI, cardiac magnetic resonance imaging; dpi, days post-infection; ECG, electrocardiogram; FA, formaldehyde treatment; hpi, hours post-infection; LV, left ventricle; n, number of inoculated animals; N, total number of animals in each experimental set; n, number of animals in each group; PFU, plaque-forming units; RV, right ventricle.

2.8 3D reconstructions of viral protein in cardiac tissue

3D localization of viral particles was performed using the Imaris Software (Bitplane AG, Switzerland). For 3D reconstructions, we used a 0.20- μ m detail level and a threshold based on absolute intensity. All images were reconstructed from a 5–10 μ m depth stacked image.

2.9 RNA extraction and PCR

RNA was isolated from myocardial samples of Mock, PAmut-, and PB2mut-infected mouse hearts using TRIzol (15596026, Thermo Fisher Scientific). cDNA was then synthesized from total RNA using the Applied Biosystems High Capacity cDNA Reverse Transcription kit (4368814, Thermo Fisher Scientific). Gene expression analysis in cardiac tissue was performed by quantitative PCR (qPCR). Then qPCR was conducted with SYBR Green (4367659, Thermo Fisher Scientific), and cDNA was amplified using DNA primers designed for every gen based on the mouse genome. Gene expression of interleukin (IL)-1 β , IL-6, lysyl oxidase, and brain natriuretic peptide were evaluated. Housekeeping

genes (GAPDH and B2M) were measured for gene expression normalization and the $2^{-\Delta\Delta C_t}$ method was used for relative gene expression quantification.

Specific primers to amplify viral NEP mRNA were designed to detect it by PCR. NEP mRNA is a spliced mRNA transcribed from the NS viral segment that is only present in cells with ongoing viral replication and transcription.²⁶

2.10 Surface ECG analysis of mice infected with influenza virus

Three groups of WT conscious mice including 10 animals per group (Mock, PB2mut, and PAmut) were used to study any potential ECG alterations during sequential follow-up (Figure 1). ECGs were recorded in the fully awake state to circumvent any potential anaesthesia-related confounding factor associated with ventilation problems. Upon inoculation (Day 0), ECG changes in conventional intervals (PR segment, QRS complex, and QT interval) were monitored daily. Three animals were euthanized on Day 1 after inoculation, two animals on Day 2, and two

animals on Day 4 to obtain ventricular samples for monitoring viral titre, western-blot, immunohistochemistry, and qPCR analyses. The remaining three animals per group at Day 4 after inoculation were used for cardiac magnetic resonance imaging (C-MRI) studies after completing the sequential follow-up of ECG parameters. Data were stored for off-line analysis using custom MatLab scripts for pre-processing, visualization, and quantification of electrophysiological intervals and heart rate variability (see [Supplementary material online, Figure S1](#)). Further technical details are described in the [Supplementary material online](#).

2.11 High-resolution cardiac magnetic resonance imaging

Nine explanted mouse hearts underwent C-MRI characterization of any overt and virus-related short-term structural damage. Four days after virus inoculation, three animals from each experimental group were euthanized after completing the last ECG follow-up ([Figure 1](#)). Five minutes before euthanasia and heart removal, a 0.2 mM/kg bolus of gadolinium-based contrast agent (Gadovist, Bayer Hispania, S.L.) was injected intravenously to ensure that gadolinium reached the whole heart. All explanted and preserved hearts underwent C-MRI using a 7-T Agilent/Varian scanner (Agilent, Santa Clara, CA, USA) equipped with a DD2 console and an actively shielded 115/60 gradient with a homemade solenoidal small coil for microimaging. The imaging protocol consisted of a 3D image (spin echo sequence, voxel resolution 31.3×70.3×31.3 μm) followed by a T1 map (inversion recovery spin echo multi-slice sequence, six slices, slice thickness: 0.5 mm). Further technical details are described in the [Supplementary material online, Figures S2–S4](#).

2.12 Statistical analyses

Student's *t*-test, two-way ANOVA, χ^2 , or the non-parametric Kruskal–Wallis test for multiple comparisons were applied as appropriate. A *P* < 0.05 was considered statistically significant. All data were analysed with GraphPad Prims v.5.00 (GraphPad Software Inc., CA, USA).

3. Results

3.1 Mice infected with influenza virus die prematurely

We previously identified a higher mortality rate for PAmut virus compared to PB2mut, CAL, and double mutant PB2/PAmut recombinant viruses.¹⁷ During the determination of the 50% lethal dose (infection with 10³, 10⁴, 10⁵, 10⁶ pfu) of these recombinant viruses, we observed that mortality of mice infected with PAmut and PB2/PAmut (dose 10⁶ pfu) occurred before reaching 75% of the original body weight that constitutes the ethical limit established for euthanasia (range: 95–77% of the original weight; [Figure 2A](#)). The data indicate that these recombinant viruses may cause premature death in some infected animals.

3.2 Human recombinant viruses are present in the hearts of infected mice

Mice infected with a previously described F-IAV virus, associated with a fatal case infection, showed certain amount of infectious particles in their heart.²⁷ These data, together with premature death documented in PAmut and PB2/PAmut-infected mice, prompted us to study the ability of human influenza virus to infect the heart. We explored the presence of IAV in hearts of mice infected with a sub-lethal dose (10³ pfu) of mutant virus and tested for heart viral titres compared with lung viral titres

in each infected animal. At 2 dpi, we found viral particles in the heart of a high proportion of all infected mice ([Figure 2B](#)), but the frequency and duration of infection were higher in PAmut-infected mice. Lung viral titres progressively increased after inoculation in all infected mice and reached the highest values at 2 dpi ([Figure 2C](#)). Lung viral titres also showed that mice infected with PAmut or PB2/PAmut had the highest viral titres at all time intervals.¹⁷ Accordingly, cardiac viral titres were detected earlier in PAmut-infected mice ([Figure 2C](#)) and remained for longer time during the 4-day follow-up period. Importantly, lung viral titres obtained with any of the recombinant viruses did not statistically correlate with viral titres in the mouse heart at any of the time intervals ([Figure 2C](#), shown *r*²). Thus, similar lung viral titres showed a wide range of heart viral titres (in [Figure 2C](#), see red and orange dots at 2 dpi and black and red dots at 4 dpi). The latter supports the notion that heart infection does not directly correlate with the extension of lung infection, and virus pathogenicity may be a more relevant factor to reach and infect the heart *in vivo*.

3.3 Influenza virus replication is present in infected hearts

The spliced viral NEP mRNA (a product of replication, [Figure 2D–G](#)) was detected in all infected hearts ('+' samples in [Figure 2F](#)) and was absent in heart samples of infected animals without heart infection ('-' samples in [Figure 2F](#)). Furthermore, the viral NP protein was found in the nucleus and cytoplasm of cardiomyocytes from infected hearts ([Figure 3A and B](#) and see [Supplementary material online, Figure S5](#) and [Videos S1 and S2](#)). Moreover, quantification of the NP signal in infected ventricular tissue showed significantly higher values in PAmut-infected hearts compared with PB2- and Mock-infected hearts ([Figure 3C](#)). This is consistent with higher viral titres in PAmut-infected hearts ([Figure 2C](#)). Further analysis of infected hearts also detected NP signal in cardiac endothelial cells ([Figure 3D](#)). These data demonstrate that human IAV can replicate in the heart of infected mice. Furthermore, virus pathogenicity and infection of the endothelial cells of blood vessels seem to be involved in viral spread from lung tissue to the heart.

3.4 Viral pathogenicity determines viral replication kinetics in cardiac cells

Direct cardiac pathogenicity and replication, independent of lung infection, was addressed using infected mouse HL-1 cardiac muscle cells with PAmut or PB2mut recombinants; or with CAL recombinant as control virus. Infection at low moi (0.001) showed significantly faster-growing kinetics and higher viral titres in PAmut-infected cells compared to PB2mut- or CAL-infected cells ([Figure 3E](#)). Interestingly, such differences were not present in lung epithelial cells infected with either PAmut or PB2mut virus (see [Supplementary material online, Figure S6](#)).¹⁷ Cells were also infected at high moi (3) with PAmut or PB2mut viruses, or were Mock-infected as control. PAmut-infected cells accumulated significantly higher levels of viral NP and PB1 proteins than attenuated PB2mut-infected cells (see [Supplementary material online, Figure S7](#)). Differences in viral kinetics were also monitored by nuclear (early infection) or cytoplasmic (late infection) localization of NP in cells infected at 5 moi using confocal immunofluorescence microscopy ([Figure 3F](#)). At 8 hpi, NP was mainly detected in the nucleus of PB2mut-infected cells and in the cytoplasm of PAmut-infected cells. Quantitative analysis showed that NP distribution was significantly different between PB2mut and PAmut viruses ([Figure 3G](#)). Altogether, the data demonstrate that human

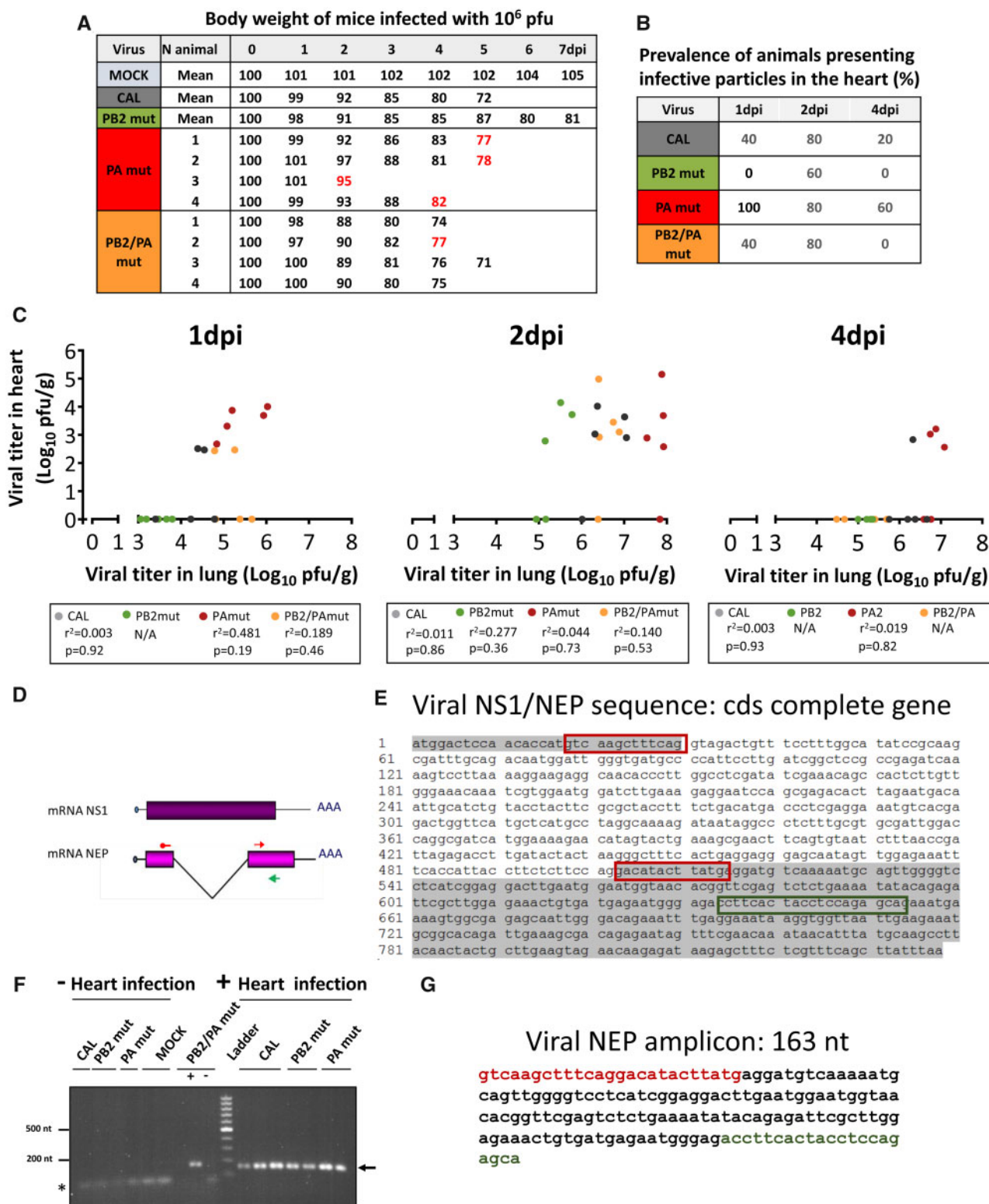


Figure 2 Premature death upon influenza A virus (IAV) infection correlates with high levels of infectious particles, active viral replication, and the presence of spliced viral NEP mRNA in the heart. BALB/c AnNHsd mice ($n = 4$) were intranasally infected with 10^6 pfu of the indicated viruses. (A) Body weights represented as percentage of body weight at inoculation (time 0). Red numbers denote body weight of animals with premature death. The experiment was performed twice and the results were similar. (B) BALB/c AnNHsd mice ($n = 5$) were intranasally infected with 10^3 pfu with the indicated viruses. Prevalence of IAV in the heart of infected animals shown as percentage of total animals. (C) Correlation of heart viral titres in each IAV-infected mouse with lung viral titres at different days post-infection (dpi). NA, not applicable, all values below detection limit in the heart. (D) Scheme of influenza virus spliced NEP mRNA and NS1 mRNA collinear to full-length NS segment. Red and green arrows indicate localization of primers used in PCR to detect NEP mRNA. (E) Sequence of the spliced NEP mRNA sequence (grey) within the full-length viral NS segment sequence. Red and green rectangles represent the sequence of forward and

IAV can infect and replicate in cardiac cells with replication kinetics directly related to virus pathogenicity.

3.5 Viral pathogenicity determines early inflammation and imbalance in extracellular matrix of infected hearts

Heart samples from PAmut-, PB2mut-, and control Mock-infected mice did not reveal any overt acute histopathologic alterations in H&E stained samples (Figure 4A). Masson Trichrome staining of heart tissue did not reveal any significant increase in cardiac fibrosis with any of the recombinant viruses at 4 days after inoculation (Figure 4B and C). Consistent with histopathology analyses, neither post-contrast T1 mapping data nor the normalized fibrosis volumes was significantly different among Mock-, PB2mut-, and PAmut-infected mice (see Supplementary material online, Table S2). Cardiac MRI-derived myocardial mass quantification was similar in infected and Mock control animals. Representative sample cases are shown in Figures S3 and S4, see Supplementary material online.

More specific analyses using qPCR revealed an early and statistically significant increase of lysyl oxidase mRNA in cardiac samples from mice infected with the highly pathogenic PAmut virus (Figure 4D). Although sequential echocardiography studies were not performed because of biosafety restrictions, Brain Natriuretic Peptide (BNP) mRNA did not significantly increase in any of the infected groups of animals (Figure 4E). Conversely, an acute pro-inflammatory response was detected in the heart of PAmut- and PB2-infected mice. More specifically, IL-1 β mRNA levels significantly increased in PAmut- and PB2-infected mice compared to Mock-infected controls (Figure 4F). IL-6 mRNA only increased significantly in mice infected with the most pathogenic PAmut virus (Figure 4G).

3.6 Influenza virus-infected mice show significant cardiac conduction alterations

Mice were infected with 10^6 pfu (dose associated with premature death in PAmut-infected animals; Figure 2A). A total of 51 820 heartbeats were included for analysis using an average of 460 ± 92 beats per ECG acquisition during the 4-day sequential follow-up. PAmut- and PB2mut-infected mice developed progressively longer RR intervals than controls (Figure 5A and B). The maximum effect of PAmut and PB2mut infection on RR intervals was observed at 2 dpi (Figure 5B). PAmut-infected mice also showed significantly longer RR intervals than PB2mut-infected mice at 2 dpi (Figure 5B). The PR interval also showed significantly longer values in PAmut- and PB2mut-infected mice at 2 dpi compared to baseline values (Figure 5C). QRS complex duration was significantly prolonged in PAmut-infected mice compared to controls at 2 dpi (Figure 5D). Corrected QT intervals were similar among groups (Figure 5E). Parallel to ECG alterations (see Supplementary material online, Table S1) and indicative of disease, body weight loss was substantially higher in PAmut- and PB2mut-infected mice compared to controls (see Supplementary material online, Figure S8A). Mortality rates were also significantly higher

in PAmut-infected mice compared to PB2mut-infected animals and controls (see Supplementary material online, Figure S8B). In the same animals, further molecular analyses showed that ATP levels in PAmut-infected mice significantly decreased compared to Mock- and PB2mut-infected mice (Figure 5F). Moreover, decreased ATP levels inversely correlated with viral titres in heart samples of those animals (Figure 5G), which further reflects the higher pathogenicity of the recombinant PAmut virus. Daily ECG recordings demonstrated that severe cardiac conduction alterations could be present at the time of premature death. This may happen in the absence of histopathologic features of coagulative necrosis or a significant increase in fibrosis, as shown in the representative case of Figure 5H.

3.7 Infected animals show active viral replication in cardiac Purkinje cells

Influenza virus infection of cardiac-specific Purkinje cells may further contribute to ECG alterations *in vivo*. Immunofluorescence and confocal microscopy analyses in excised hearts (see Supplementary material online, Figure S9) from PAmut- and PB2mut-infected Cx40^{eGFP} transgenic mice identified the NP protein in both the cytoplasm and the nucleus of Purkinje cells (Figure 6A and see Supplementary material online, Videos S3 and S4). This indicates also active viral replication in the cardiac-specific conduction system. As reported in infected WT animals, histopathology analysis did not show overt relevant alterations in H&E and Masson Trichrome ($n = 3$ per group, median fibrosis: 0.03%, 0.04%, and 0.01% for Mock-, PB2mut- and PAmut-infected animals, respectively) stained samples (Figure 6B and C).

3.8 Human-induced pluripotent stem cell-derived cardiomyocytes as a model for human heart infection

Consistent with the data obtained in HL-1 cardiac cells and in the mouse heart, hiPSC-CMs were also susceptible to human IAV infection. At 12 hpi, after 3 moi infection, viral PB1 accumulation levels were significantly higher in PAmut-infected cells than in attenuated PB2mut-infected ones (Figure 7A and B). Moreover, YM1E1 protease, an indicator of mitochondrial integrity,^{28,29} significantly decreased in infected cells. The latter was also more exacerbated in PAmut-infected cells compared to PB2mut-infected ones (Figure 7C and D). This was also consistent with the decrease in ATP levels documented in infected mice hearts (Figure 5F). Further analysis of the underlying causes associated with the electrophysiological phenotype *in vivo* showed that Kir2.1 levels did not significantly change among the infected groups (Figure 7E and F), consistent with non-significant changes in the QT interval *in vivo* (Figure 5E). Conversely, Cx43 and NaV1.5 levels decreased in influenza virus-infected cells, especially in the highly pathogenic PAmut infection (Figure 7E, G, and H), which was also consistent with QRS complex prolongation *in vivo* (Figure 5D).

Figure 2 Continued

reverse primers used for amplification of spliced NEP mRNA, respectively. (F) Agarose gel with amplified NEP mRNA in heart samples of CAL-, PB2mut-, PAmut-, or PB2/PAmut-infected mice obtained at 2 dpi (at time of the highest viral titres in panel D). + indicates samples showing infectious viral particles. - indicates samples not showing infectious viral particles as determined by plaque assay (B and C). Arrow bands corresponding to spliced NEP mRNA. The asterisk indicates dimer primers. (G) Sequence of the obtained amplicons.

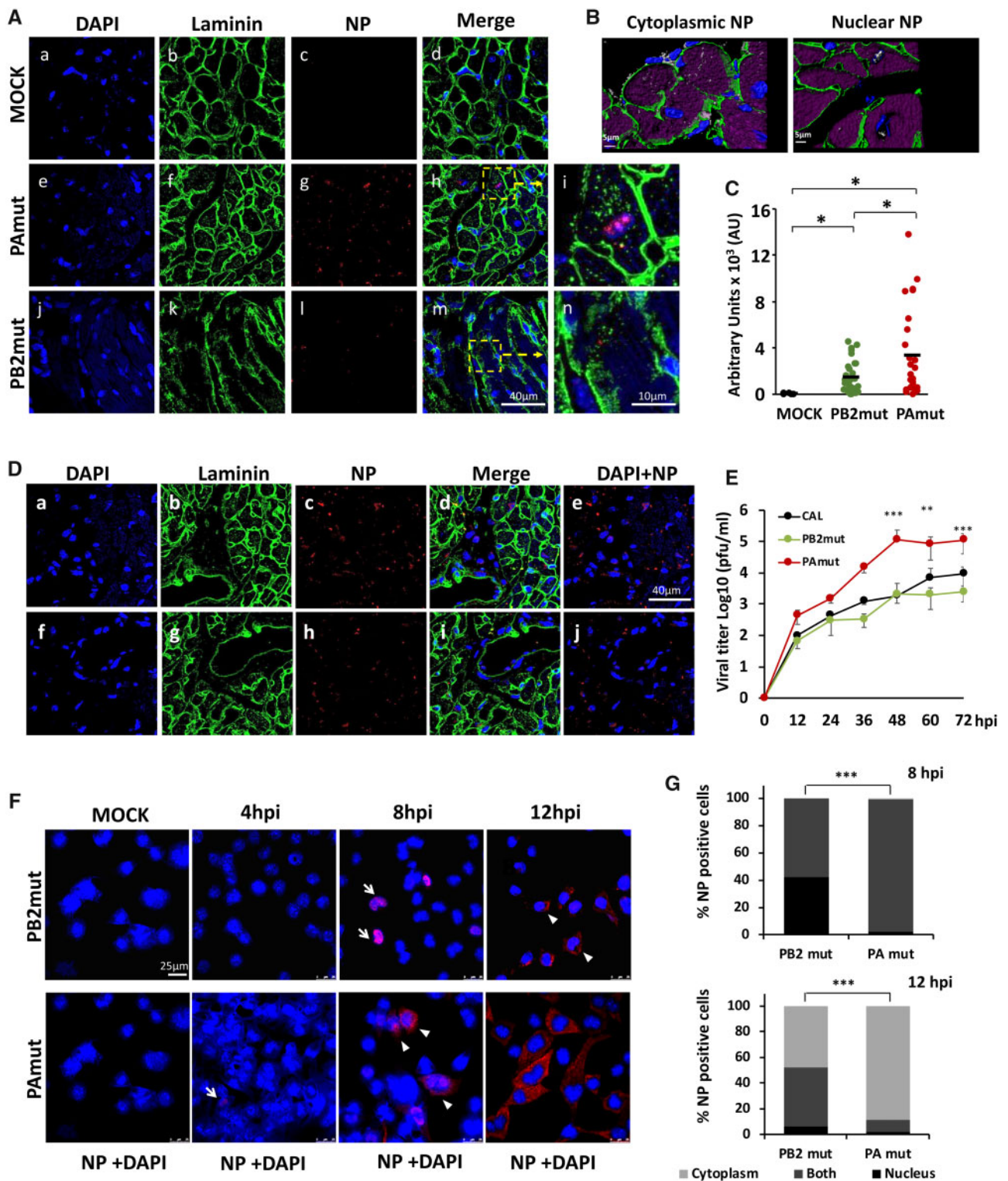
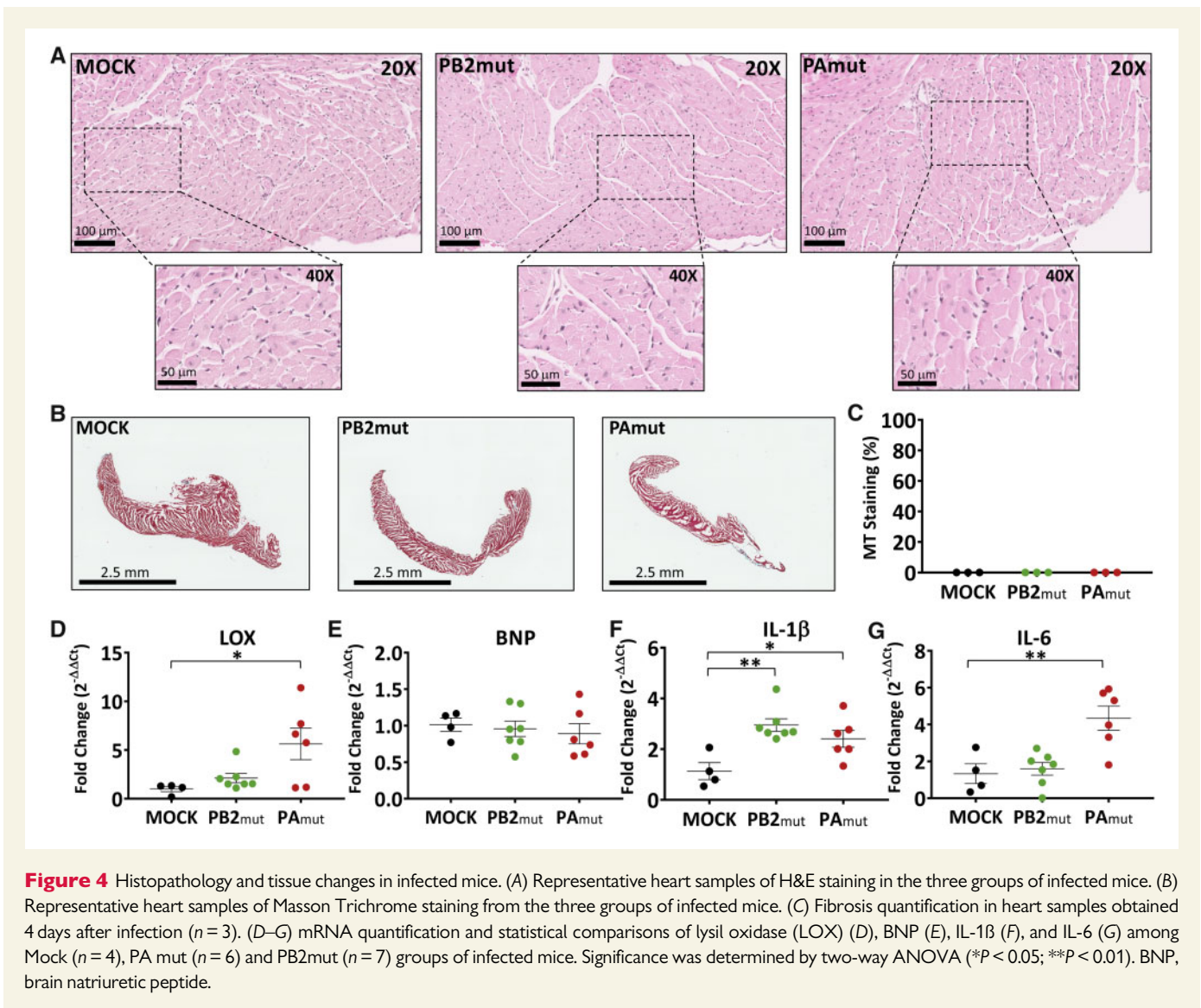


Figure 3 Active replication of influenza A virus in cardiac tissue. PAmut virus replicates faster than attenuated PB2mut virus in HL-1 cells. (A) Detection of viral nucleoprotein (NP) by confocal microscopy of immunofluorescences in heart tissue from control animals (MOCK; upper panels, *a–d*), PAmut virus- (middle panels, *e–i*) or PB2mut virus- (lower panels, *j–n*) infected animals. The boxed areas in merged images (*h* and *m*) are shown enlarged in the insets (*i* and *n*). (B) 3D reconstructions of cytoplasmic (left panel) or nuclear (right panel) NP viral protein in PAmut-infected heart tissue (see [Supplementary material online](#), *Videos S1 and S2*). Magenta, auto-fluorescence in cardiomyocytes; NP viral protein is shown in white for better visualization in 3D reconstructions. (C) Quantification of NP signal in infected heart tissues at 2-day post-infection (dpi). A minimum of 27 images from two different hearts have been quantified for each group. * $P < 0.05$ by Student's *t*-test. (D) Detection of viral NP in endothelial cells surrounding a heart blood vessel from animals infected with PAmut virus. (E) Viral replication kinetics of control CAL, PAmut, or PB2mut virus in cultured HL-1-infected cells (10^{-3} multiplicity of infection, moi). Experiments were performed in triplicates. Significance was determined by two-way ANOVA with Bonferroni post hoc test (* $P < 0.05$; ** $P < 0.01$;



4. Discussion

We report that both pathogenic and attenuated human IAVs can infect cardiomyocytes and Purkinje cells in the mouse heart without correlation with lung viral titres. The infection was also present in cardiac endothelial cells, which represent a potential pathway for viral transmission from lung to heart tissue. The highly pathogenic recombinant PAmut virus replicates more rapidly in mouse cardiomyocyte cultures and induces an early increase in inflammatory cytokines with overt signs of bradycardia and abnormal cardiac impulse propagation *in vivo* that may lead to premature death. The electrophysiological phenotype *in vivo* was

associated with an acute decrease in Cx43 and Na_v1.5 levels, and overt mitochondrial dysfunction in infected hiPSC-CMs. The results indicate that direct heart infection may have important implications in human influenza virus outbreaks, in addition to the indirect effects derived from respiratory pathology. The latter is consistent with clinical reports of severe cardiac complications in infected patients, even without apparent respiratory damage.^{13,14}

Multiple reports have indicated a temporal relationship of influenza outbreaks with acute coronary events and increased mortality in the elderly.^{3,30,31} Recently, Kwong et al.³² have documented an increased incidence of acute myocardial infarction within 7 days after detection of IAV

Figure 3 Continued

*** $P < 0.001$). (F) At indicated hours post-infection (hpi), samples of Mock-, PB2mut- or PAmut-infected HL-1 cells (moi 5) were used for immunofluorescence confocal microscopy. Arrows and arrowheads indicate nuclear and cytoplasmic localization of NP protein, respectively. Experiments were performed in triplicates. (G) Distribution of nuclear, cytoplasmic, or both localizations of NP viral protein within 100% of positive PB2mut- or PAmut-infected cells at 8 hpi (top) and 12 hpi (bottom). A minimum of 160 cells from three independent experiments were analysed for PB2mut or PAmut virus at each time point. Significance was determined by χ^2 test (*** $P < 0.001$). Blue, nucleus staining (DAPI); green, laminin; red, NP viral protein (but white, C).

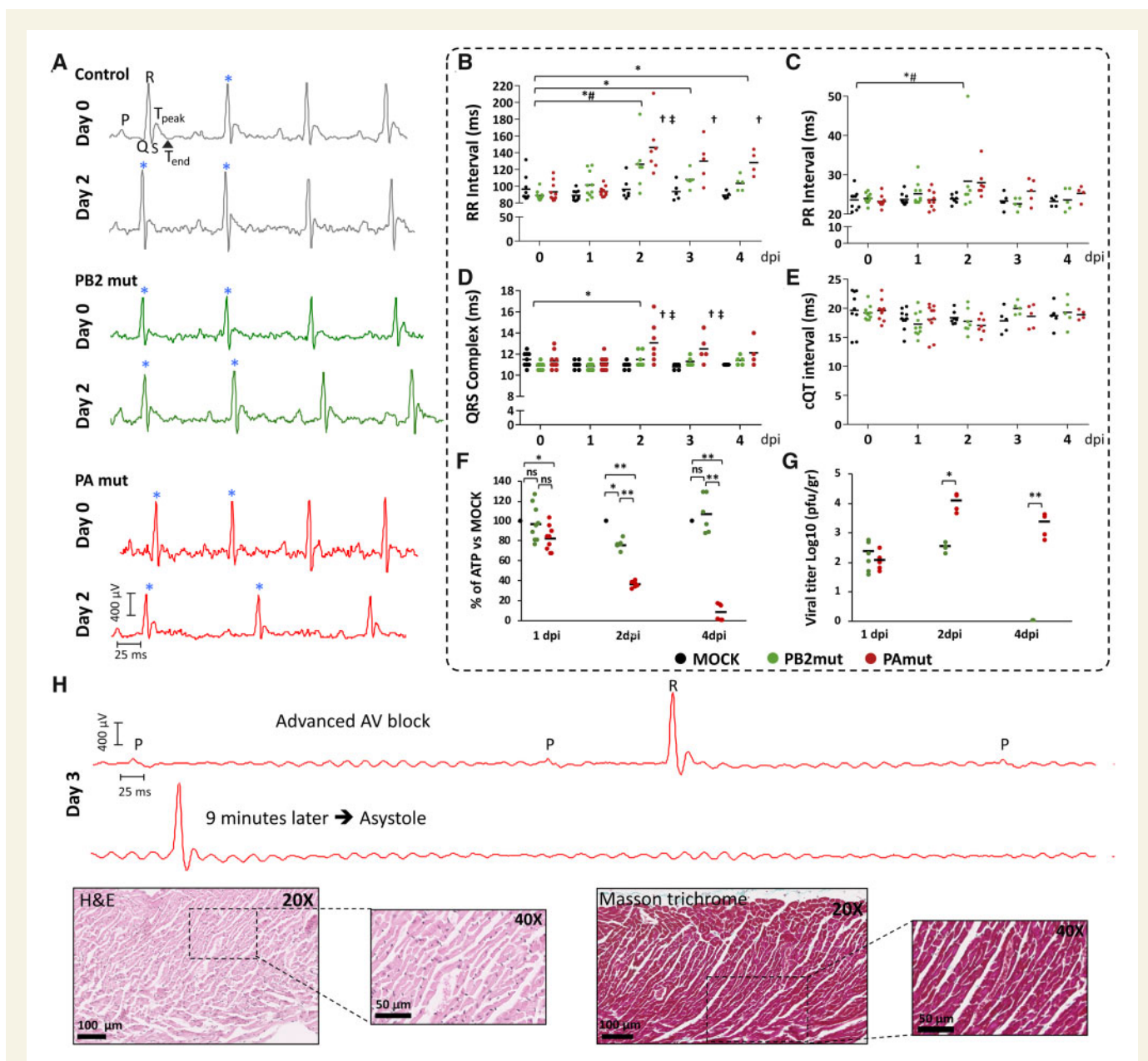


Figure 5 ECG alterations in mice infected with influenza virus. (A) Randomly selected tracings from control, PB2mut, and PAmut mice at Days 0 and 2 after virus inoculation. The tracings show overt prolongation of RR intervals (slower heart rate) and PR intervals in PAmut-infected mice at Day 2. Blue asterisks indicate R waves. (B–E) Surface ECG-based quantification of cardiac rhythm and conduction alterations in virus-infected animals and control mice. *, #, †, and ‡ show $P < 0.05$ for PAmut vs. PAmut Day0 (*), PB2mut vs. PB2mut Day0 (#), PAmut vs. controls at that time point (†), and PB2mut vs. controls at that time point (‡). Animals ($n = 10$) were intranasally infected with 10^6 pfu of PB2mut, or PAmut recombinant virus or were Mock-infected, and were sequentially euthanized for collection of samples. Number of animals for comparisons: Days 0, 1: $n = 10$ (PB2 and PA) and $n = 9$ (Mock. The 10th animal was excluded due to poor signal quality); Day 2: $n = 7$ per group; Day 3: $n = 5$ per group; and Day 4: $n = 5$ (PB2, Mock) and $n = 4$ (PA. The fifth animal died on Day 3). Significance was determined by two-way repeated-measures ANOVA with Bonferroni post hoc test (* $P < 0.05$; ** $P < 0.01$). (F) ATP levels were evaluated in triplicates in total heart extracts at 1- ($n = 3$), 2- ($n = 2$), and 4- ($n = 2$) day post-infection (dpi). Mock data are shown as 100% in one dot. (G) Viral titres were determined in hearts of the same infected animals at indicated dpi and were evaluated in duplicates (1 dpi, $n = 3$; 2 dpi, $n = 2$; 4 dpi, $n = 2$, per group). In (F) and (G), significance was determined by Student's t -test (ns: not significant, * $P < 0.05$, ** $P < 0.01$). (H) Representative ECG alterations in a PAmut-infected mouse before dead. Haematoxylin and eosin (H&E) and Masson trichrome staining from the same animal.

infection. In fact, during influenza epidemics, people with cardiovascular disease are particularly at risk of events, and annual influenza virus immunization is currently recommended in adults with cardiovascular disease.³³ Moreover, clinical evidence indicates that influenza vaccination may protect against acute myocardial infarction.^{34,35}

Despite the association between influenza virus infection and cardiovascular events, influenza virus antigens or RNAs have only rarely been noticed in the myocardium. Viral RNA was detected in a myocardial biopsy of a young woman with fulminant myocarditis and cardiogenic shock.³⁶ Viral antigens have been also detected in cardiomyocytes from

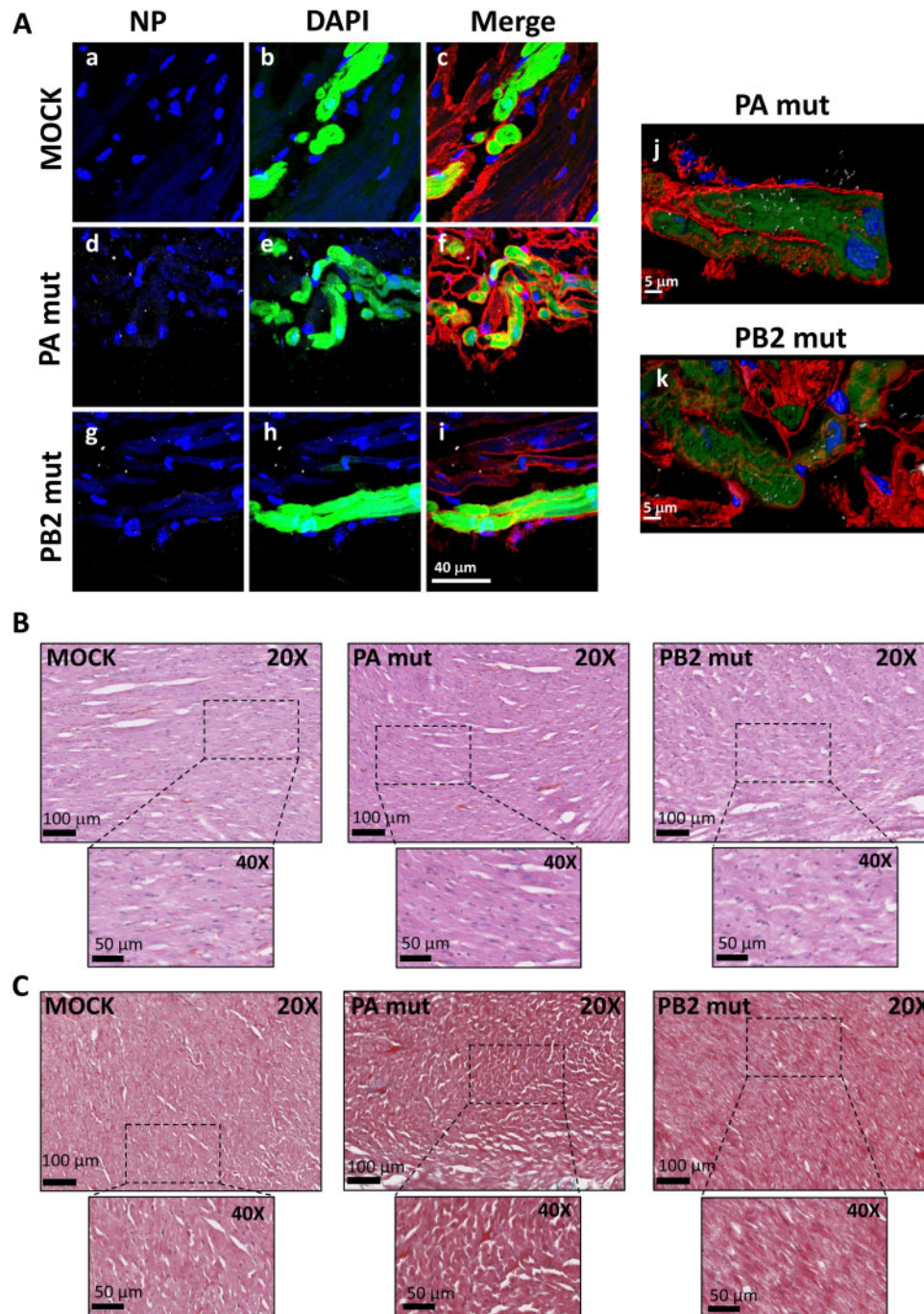


Figure 6 Active replication of influenza A virus in Purkinje cells. (A) Detection of the NP viral protein using immunofluorescence confocal microscopy in heart tissue from Cx40^{eGFP} MOCK-infected mice (upper panels, a–c) and animals infected with 10⁶ pfu of either PAmut virus (middle panels, d–f) or PB2mut virus (lower panels, g–i). Right panels (j–k) show 3D reconstructions of the NP viral protein in Purkinje cells of PAmut- (j) or PB2mut-infected hearts (k) from Cx40^{eGFP} animals (see also [Supplementary material online, Videos S3 and S4](#)). Blue, nuclear staining (DAPI); green, GFP; red, laminin; white, NP viral protein staining. (B and C) H&E staining (B) and Masson Trichrome staining (C) of representative heart samples from Cx40^{eGFP}-infected mice.

another patient with fulminant myocarditis.¹⁴ Endomyocardial biopsies in a large series of patients with myocarditis have identified IAV RNA in five patients.³⁷ These clinical data and more dramatic reports describing the association between IAV infection and sudden cardiac death suggest that rather than a non-pathogenic viral RNA detection, concomitant to pulmonary infection, IAV identification in the myocardium may represent

a highly pathogenic scenario that may determine clinical outcomes.^{13,15,38} A recent report by Kenney et al.³⁹ have shown that influenza virus replication in the heart and virus-related mortality dramatically increased in knockout mice with antiviral restriction factor IFN-induced transmembrane protein 3 (IFITM3) deficiency. These authors used a mouse-adapted influenza virus strain that caused cardiac

rhythm alterations and early activation of profibrotic and inflammatory pathways. Our results provide new evidence of IAV virus replication in heart tissue using human recombinant viruses carrying highly pathogenic (PAmut) and attenuated (PB2mut) mutations present in a virus isolated from a fatal-patient case infected during the 2009 pandemic.¹⁷ Moreover, our data show that heart infection and viral titres do not correlate with lung viral titres, which supports the notion that rather than a consequence of respiratory damage, cardiac complications may also relate to virus pathogenicity and independent replication in the myocardium and specific cardiac conduction systems.

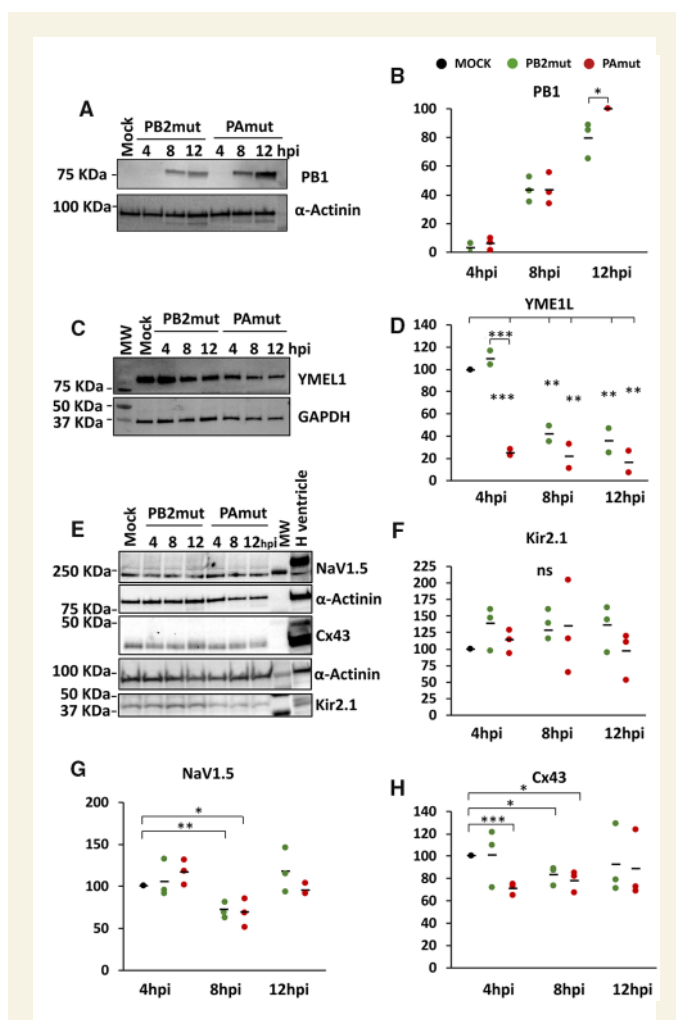


Figure 7 Influenza A virus replication and electrophysiological phenotype of infected hiPSC-CMs. hiPSC-CMs were Mock-infected or infected with the indicated virus (3 moi). Samples were used to detect the indicated proteins by western blot at the specified hours post-infection (hpi). (A) Viral PB1 protein. (C) Mitochondrial protease YME1L1. (E) Kir2.1 and NaV1.5 ion channels and Connexin43. GAPDH or α -actinin were used as loading control and healthy human ventricle tissue (H—ventricle) was loaded as human ion channels and Connexin43 control. MW denotes molecular weight markers. The experiment was performed in triplicates (duplicates for YME1L1); one representative sample is shown. Mock data are shown as 100% in one dot. B, D, F, G, and H indicate protein quantification and statistically significant analysis (* $P < 0.05$, ** $P < 0.01$, *** $P < 0.001$ by the Student's *t*-test). moi, multiplicity of infection.

The higher pathogenicity of the recombinant PAmut virus may be related to the fact that this virus accumulates low amounts of defective viral genomes, which induces a lower antiviral response in cultured cells and a higher lung inflammation compared with the PB2mut.¹⁷ Interestingly, such a reduced activation of the antiviral state might imply a delay in the immune response of infected animals, which may enable the virus to grow and disseminate uncontrolled for a short time, sufficient to infect the heart tissue. Consistent with such a hypothesis, we found infectious particles in 100% of the hearts from PAmut-infected mice at 1 dpi (Figure 2B). The deficiency in the antiviral restriction factor IFITM3, recently associated with enhanced pathogenesis and viral replication in the heart of infected mice,³⁹ reinforce the antiviral response-related pathogenicity of the PAmut virus. Moreover, the recombinant PAmut virus replicated faster than the PB2mut in cardiac cultured cells, and generated larger ECG alterations and acute mitochondrial dysfunction compared with the attenuated PB2mut. Altogether the data indicate that the specific PA D529N mutation, present in a human fatal case virus, provides an advantage for virus dissemination and replication in the myocardium. Therefore, it seems reasonable that, rather than being an indirect consequence of respiratory damage upon infection with highly pathogenic IAVs, a delay in the early immune response facilitates direct cardiac infection and early myocardial damage.

Possible explanations for the scarce detection of viral determinants in cardiac tissue of infected patients could be a low capability of the majority of influenza virus strains to infect cardiac cells and/or low levels of viral replication in heart tissue. Upregulation of specific proteases capable of cleaving influenza virus HA in the mouse heart and in H9c2 rat cardiomyocytes has been associated with the capacity of IAVs to propagate in the heart.⁴⁰ Here, we demonstrate the ability of human H1N1 IAV to infect and replicate in heart tissue of infected mice, HL-1 cardiac cells and hiPSC-CMs. Although all the tested recombinant viruses infected the heart (Figure 2), including the attenuated virus PB2mut, differences in pathogenicity correlated with cardiac virus infection capacity and replication. ECG alterations and underlying molecular changes (Figures 5 and 7) were also consistent with virus pathogenicity. Interestingly, IAV infection of HL-1 cells showed significantly faster-growing kinetics and higher viral titres in PAmut-infected cells compared to PB2mut- or control WT CAL-infected cells. However, such differences were not present in lung epithelial cells (see Supplementary material online, Figure S6), which highlights the relevance of virus pathogenicity to replicate in cardiac tissue.

The *in vivo* mouse electrophysiological phenotype showed that PAmut- and PB2mut-infected mice developed acute progressive bradycardia. Bradycardia has been also reported by Kenney *et al.*³⁹ using a mouse-adapted influenza virus strain. Here, we also report that the most pathogenic strain (i.e. PAmut) significantly affected the PR interval and QRS complex duration. Interestingly, conduction abnormalities and high-degree atrio-ventricular block have been documented also in human cases of myocarditis associated with influenza A virus infection.¹⁴ In addition, an early inflammatory state was also present in the heart of infected mice. Moreover, ECG alterations and pro-inflammatory cytokines were consistent with higher viral titres and higher viral replication in the heart of PAmut-infected mice compared to PB2mut- and Mock-infected animals. Further molecular studies in infected hiPSC-CMs also showed consistent alterations in ion channel expression and mitochondrial dysfunction, which were more evident in PAmut-infected cells. Interestingly, YME1L1 has been involved in mitochondria dynamics,²⁸ heart failure,⁴¹ maintenance of mitochondrial structure, and respiratory chain biogenesis, and stresses the relevance of correct proteostasis for mitochondrial integrity.⁴² Accordingly, the M2 protein of influenza virus

(a viroprotein) causes alteration of mitochondrial morphology, dissipation of mitochondrial membrane potential, and cell death⁴³ (reviewed in Refs^{44,45}). Altogether, the data support a heart mitochondrial damage observed upon human IAV infection (Figure 7C and D), consistently with ATP decrease, especially in the highly pathogenic PAmut virus (Figure 5F).

In the clinic, ventricular arrhythmia leading to sudden cardiac death may be also a fatal consequence of fulminant myocarditis associated with influenza A infection.¹³ In mice, we have not documented ventricular arrhythmic events in any of the infected groups of mice. Conversely, we have documented severe bradycardia and conduction abnormalities in one PAmut-infected mouse at the time of premature death 3 days after infection. However, myocarditis-related ventricular arrhythmia is a rare phenomenon in infected patients, which may also be the case in mice. In addition, we did not have the possibility of obtaining continuous ECG recordings under biosafety level 2+ conditions, which has also affected our ability to record ventricular arrhythmia. Notwithstanding such different rhythm alterations reported in the clinic, the ability of the virus to infect cardiac tissue makes it a potential hazard.^{13–15,38} Here, we report that this is especially relevant for viral strains of high pathogenicity. Fortunately, there are clinical reports of influenza-induced fulminant myocarditis successfully treated with intravenous peramivir.^{46,47} Therefore, new studies are warranted to investigate the potential value of antiviral therapies in cases with heart infection in the clinic.

4.1 Limitations

Biosafety restrictions did not allow performing echocardiography studies in mice undergoing sequential ECG monitoring. Histopathology analysis did not show immune cell infiltration at 4-day post-infection, which may be consistent with sequential findings of viral myocarditis in mice models; with an initial increase in inflammatory cytokines prior to inflammatory cell infiltration that would be predominantly evident at day 5 post-infection.⁴⁸

5. Conclusions

Human IAV can infect the heart and cardiac-specific conduction system, which may contribute to virus-related cardiac complications and premature death in the clinic.

Supplementary material

Supplementary material is available at *Cardiovascular Research* online.

Authors' contributions

J.V., A.N., and A.F. contributed to the design acquisition, analysis, and interpretation of all viral inoculation and viral growth studies in cell culture and in vivo. N.Z. and C.G. contributed to the acquisition, analysis, and interpretation of the studies performed in cell-cultured cardiomyocytes. D.F.-R., J.J., and S.N.N. contributed to the design acquisition, analysis, and interpretation of the ECG and cardiac imaging data. J.M.-A.-A. contributed to the analysis of fibrosis and inflammation data. A.F., N.Z., and A.N. contributed to the design acquisition, analysis, and interpretation of hiPSCs infection. A.B. and C.P.C., contributed to software development and analysis of ECG and cardiac imaging data. J.A.N.-A. and A.H. contributed to the design acquisition and analysis of immunofluorescence

microscopy and histology images. D.C., M.D., and J.R.-C. contributed to the design of cardiac imaging protocols and acquisition of cardiac magnetic resonance images. A.F., D.P.C., and G.G.-S. contributed to the design acquisition and analysis Purkinje fibres infection. A.N., J.J., and J.V. contributed to drafting and revising the article. A.F. supervised the studies. D.F.-R. and A.F. wrote the article.

Acknowledgements

We are indebted to Dr Antonio Bernad for scientific advice at CNB-CSIC, and Dr Daniel Goldstein for animal experiments support at the University of Michigan, USA. We are grateful to Dr Juan Ortín for critical comments on the article. We thank Susana Cañon and Diego Herrero for their advice on HL-1 cells management and Silvia Marquez-Jurado for reagents and advice. We also acknowledge the technical assistance and advice of Sylvia Gutiérrez, CNB Advanced Light Microscopy Unit (CNB-CSIC), Oscar Sanchez, Soledad Montalbán, and Histology Service (CNB-CSIC). We thank the Cardiovascular Regeneration Core Laboratory and André Monteiro da Rocha, Yan Chen, Ede Fortune, Sherri Wood and Candide Smith for their helpful assistance at the University of Michigan.

Conflict of interest: none declared.

Funding

J.V. is a PhD fellow of the La Caixa Foundation International Fellowship Programme (La Caixa/CNB). This work was supported by the European Molecular Biology Organization (STF-7649 to A.F.), the Spanish Ministry of Science, Innovation and Universities (MCIU), (BFU2014-57797-R and BFU2017-83392-R to A.N.), and the network Ciber de Enfermedades Respiratorias (CIBERES) including the Improvement and Mobility Programme. CNB-CSIC is supported by the Maria de Maeztu Units of Excellence Program from the Spanish State Research Agency. CNIC is a Severo Ochoa Center of Excellence (SEV-2015-0505). CNIC is supported by MCIU and the Pro CNIC Foundation. CIC biomaGUNE is supported by the Maria de Maeztu Units of Excellence Program from the Spanish State Research Agency – Grant No. MDM-2017-0720. This study was supported by grants from Fondo Europeo de Desarrollo Regional (CB16/11/00458), grants SAF2015-65607-R and SAF2016-80324-R from MCIU (A.H. and D.F.-R.) and fellowship SVP-2014-068595 to J.A.N.-A. This study was supported by Frankel Cardiovascular Centre, Michigan Medicine (Grant No. 332475). J.J. is supported in part by the National Heart, Lung, and Blood Institute (R01 Grant No. HL122352). S.F.N. is supported in part by the National Heart, Lung, and Blood Institute (Grant Nos R21HL138064 and R01HL129136).

References

1. Neumann G, Noda T, Kawaoka Y. Emergence and pandemic potential of swine-origin H1N1 influenza virus. *Nature* 2009;**459**:931–939.
2. Hsieh YC, Wu TZ, Liu DP, Shao PL, Chang LY, Lu CY, Lee CY, Huang FY, Huang LM. Influenza pandemics: past, present and future. *J Formos Med Assoc* 2006;**105**:1–6.
3. Collins SD. Excess mortality from causes other than influenza and pneumonia during influenza epidemics. *Public Health Rep* 1932;**47**:2159–2179.
4. Jeyanathan T, Overgaard C, McGeer A. Cardiac complications of influenza infection in 3 adults. *CMAJ* 2013;**185**:581–584.
5. Warren-Gash C, Hayward AC, Hemingway H, Denaxas S, Thomas SL, Timmis AD, Whitaker H, Smeeth L. Influenza infection and risk of acute myocardial infarction in England and Wales: a CALIBER self-controlled case series study. *J Infect Dis* 2012;**206**:1652–1659.
6. Madjid M, Miller CC, Zarubaev VV, Marinich IG, Kiselev OI, Lobzin YV, Filippov AE, Casscells SW III. Influenza epidemics and acute respiratory disease activity are associated with a surge in autopsy-confirmed coronary heart disease death: results from 8 years of autopsies in 34,892 subjects. *Eur Heart J* 2007;**28**:1205–1210.
7. Clayton TC, Capps NE, Stephens NG, Wedzicha JA, Meade TW. Recent respiratory infection and the risk of myocardial infarction. *Heart* 2005;**91**:1601–1602.

8. Mamas MA, Fraser D, Neyses L. Cardiovascular manifestations associated with influenza virus infection. *Int J Cardiol* 2008;**130**:304–309.
9. Puzelli S, Buonaguro FM, Facchini M, Palmieri A, Calzoletti L, De Marco MA, Arace P, de Campora E, Esposito C, Cassone A, Rezza G, Donatelli I; Surveillance Group for Pandemic H1N1v, Campania HNTF. Cardiac tamponade and heart failure due to myopericarditis as a presentation of infection with the pandemic H1N1 2009 influenza A virus. *J Clin Microbiol* 2010;**48**:2298–2300.
10. Ukimura A, Satomi H, Ooi Y, Kanzaki Y. Myocarditis associated with influenza A H1N1pdm2009. *Influenza Res Treat* 2012;**2012**:1–8.
11. Chacko B, Peter JV, Pichamuthu K, Ramakrishna K, Moorthy M, Karthik R, John G. Cardiac manifestations in patients with pandemic (H1N1) 2009 virus infection needing intensive care. *J Crit Care* 2012;**27**:106 e101–e106.
12. Corrales-Medina VF, Madjid M, Musher DM. Role of acute infection in triggering acute coronary syndromes. *Lancet Infect Dis* 2010;**10**:83–92.
13. Gdynia G, Schnitzler P, Brunner E, Kandolf R, Blaker H, Daum E, Schnabel P, Schirmacher P, Roth W. Sudden death of an immunocompetent young adult caused by novel (swine origin) influenza A/H1N1-associated myocarditis. *Virchows Arch* 2011;**458**:371–376.
14. Miura M, Asaumi Y, Wada Y, Ogata K, Sato T, Sugawara T, Yano M, Mitsu-Oka M, Takai O, Ota K, Namiki K, Sato D, Sato E, Nagura H, Kimura T. A case of influenza subtype A virus-induced fulminant myocarditis: an experience of percutaneous cardio-pulmonary support (PCPS) treatment and immunohistochemical analysis. *Tohoku J Exp Med* 2001;**195**:11–19.
15. Komai T, Nakazawa G, Asai S, Ikari Y. Fatal fulminant myocarditis associated with novel influenza A (H1N1) infection. *Eur Heart J* 2011;**32**:283–283.
16. Guan X, Yang W, Sun X, Wang L, Ma B, Li H, Zhou J. Association of influenza virus infection and inflammatory cytokines with acute myocardial infarction. *Inflamm Res* 2012;**61**:591–598.
17. Vasilijević J, Zamarreño N, Oliveros JC, Rodríguez-Frandsen A, Gómez G, Rodríguez G, Pérez-Ruiz M, Rey S, Barba I, Pozo F, Casas I, Nieto A, Falcón A. Reduced accumulation of defective viral genomes contributes to severe outcome in influenza virus infected patients. *PLoS Pathog* 2017;**13**:e1006650.
18. Ponce-Balbuena D, Guerrero-Serna G, Valdivia CR, Caballero R, Diez-Guerra FJ, Jiménez-Vázquez EN, Ramírez RJ, Monteiro da Rocha A, Herron TJ, Campbell KF, Willis BC, Alvarado FJ, Zarzoso M, Kaur K, Pérez-Hernández M, Matamoros M, Valdivia HH, Delpón E, Jalife J. Cardiac Kir2.1 and NaV1.5 channels traffic together to the sarcolemma to control excitability. *Circ Res* 2018;**122**:1501–1516.
19. Jorba N, Coloma R, Ortín J. Genetic trans-complementation establishes a new model for influenza virus RNA transcription and replication. *PLoS Pathog* 2009;**5**:e1000462.
20. Gonzalez S, Ortín J. Distinct regions of influenza virus PB1 polymerase subunit recognize vRNA and cRNA templates. *EMBO J* 1999;**18**:3767–3775.
21. Falcón AM, Marión RM, Zürcher T, Gómez P, Portela A, Nieto A, Ortín J. Defective RNA replication and late gene expression in temperature-sensitive influenza viruses expressing deleted forms of the NS1 protein. *J Virol* 2004;**78**:3880–3888.
22. Baer A, Kehn-Hall K. Viral concentration determination through plaque assays: using traditional and novel overlay systems. *J Vis Exp* 2014;**93**:e52065.
23. Miquerol L, Meysens S, Mangoni M, Bois P, van Rijen HV, Abran P, Jongsma H, Nargeot J, Gros D. Architectural and functional asymmetry of the His-Purkinje system of the murine heart. *Cardiovasc Res* 2004;**63**:77–86.
24. Rodríguez A, Pérez-González A, Nieto A. Influenza virus infection causes specific degradation of the largest subunit of cellular RNA polymerase II. *J Virol* 2007;**81**:5315–5324.
25. Hou L, Liu K, Li Y, Ma S, Ji X, Liu L. Necrotic pyknosis is a morphologically and biochemically distinct event from apoptotic pyknosis. *J Cell Sci* 2016;**129**:3084–3090.
26. Lamb RA, Choppin PW, Chanock RM, Lai CJ. Mapping of the two overlapping genes for polypeptides NS1 and NS2 on RNA segment 8 of influenza virus genome. *Proc Natl Acad Sci U S A* 1980;**77**:1857–1861.
27. Rodríguez A, Falcon A, Cuevas MT, Pozo F, Guerra S, Garcia-Barreno B, Martinez-Orellana P, Perez-Brena P, Montoya M, Melero JA, Pizarro M, Ortín J, Casas I, Nieto A. Characterization in vitro and in vivo of a pandemic H1N1 influenza virus from a fatal case. *PLoS One* 2013;**8**:e53515.
28. Ruan Y, Li H, Zhang K, Jian F, Tang J, Song Z. Loss of Yme1L perturbs mitochondrial dynamics. *Cell Death Dis* 2013;**4**:e896.
29. Richter F, Dennerlein S, Nikolov M, Jans DC, Naumenko N, Aich A, MacVicar T, Linden A, Jakobs S, Urlaub H, Langer T, Rehling P. ROMO1 is a constituent of the human presequence translocase required for YME1L protease import. *J Cell Biol* 2019;**218**:598–614.
30. Warren-Gash C, Smeeth L, Hayward AC. Influenza as a trigger for acute myocardial infarction or death from cardiovascular disease: a systematic review. *Lancet Infect Dis* 2009;**9**:601–610.
31. Nguyen JL, Yang W, Ito K, Matte TD, Shaman J, Kinney PL. Seasonal influenza infections and cardiovascular disease mortality. *JAMA Cardiol* 2016;**1**:274–281.
32. Kwong JC, Schwartz KL, Campitelli MA, Chung H, Crowcroft NS, Karnauchow T, Katz K, Ko DT, McGeer AJ, McNally D, Richardson DC, Rosella LC, Simor A, Smieja M, Zahariadis G, Gubbay JB. Acute myocardial infarction after laboratory-confirmed influenza infection. *N Engl J Med* 2018;**378**:345–353.
33. Davis MM, Taubert K, Benin AL, Brown DW, Mensah GA, Baddour LM, Dunbar S, Krumholz H. Influenza vaccination as secondary prevention for cardiovascular disease: a science advisory from the American Heart Association/American College of Cardiology. *J Am Coll Cardiol* 2006;**48**:1498–1502.
34. MacIntyre CR, Mahimbo A, Moa AM, Barnes M. Influenza vaccine as a coronary intervention for prevention of myocardial infarction. *Heart* 2016;**102**:1953–1956.
35. Hsu SY, Chen FL, Liaw YP, Huang JY, Nfor ON, Chao DY. A matched influenza vaccine strain was effective in reducing the risk of acute myocardial infarction in elderly persons: a population-based study. *Medicine* 2016;**95**:e2869.
36. Montcriol A, Wiramus S, Ribeiri A, Attard N, Nait-Saidi L, Kerbaul F, Chiche L. Successful management of influenza A associated fulminant myocarditis: mobile circulatory support in intensive care unit: a case report. *Cases J* 2008;**1**:46.
37. Bowles NE, Ni J, Kearney DL, Pauschinger M, Schultheiss HP, McCarthy R, Hare J, Bricker JT, Bowles KR, Towbin JA. Detection of viruses in myocardial tissues by polymerase chain reaction: evidence of adenovirus as a common cause of myocarditis in children and adults. *J Am Coll Cardiol* 2003;**42**:466–472.
38. Cioc AM, Nuovo GJ. Histologic and in situ viral findings in the myocardium in cases of sudden, unexpected death. *Mod Pathol* 2002;**15**:914–922.
39. Kenney AD, McMichael TM, Imas A, Chesarino NM, Zhang L, Dorn LE, Wu Q, Alfaour O, Amari F, Chen M, Zani A, Chemudupati M, Accornero F, Coppola V, Rajaram MVS, Yount JS. IFITM3 protects the heart during influenza virus infection. *Proc Natl Acad Sci U S A* 2019;**116**:18607–18612.
40. Pan HY, Yamada H, Chida J, Wang S, Yano M, Yao M, Zhu J, Kido H. Up-regulation of ectopic trypsin in the myocardium by influenza A virus infection triggers acute myocarditis. *Cardiovasc Res* 2011;**89**:595–603.
41. Guo Y, Wang Z, Qin X, Xu J, Hou Z, Yang H, Mao X, Xing W, Li X, Zhang X, Gao F. Enhancing fatty acid utilization ameliorates mitochondrial fragmentation and cardiac dysfunction via rebalancing optic atrophy 1 processing in the failing heart. *Cardiovasc Res* 2018;**114**:979–991.
42. Cesnekova J, Rodinova M, Hansikova H, Zeman J, Stiburek L. Loss of mitochondrial AAA proteases AFG3L2 and YME1L impairs mitochondrial structure and respiratory chain biogenesis. *Int J Mol Sci* 2018;**19**:3930.
43. Ilyinskii PO, Gabai VL, Sunyaev SR, Thoidis G, Shneider AM. Toxicity of influenza A virus matrix protein 2 for mammalian cells is associated with its intrinsic proton-channeling activity. *Cell Cycle* 2007;**6**:2043–2047.
44. Gonzalez ME, Carrasco L. Viroproins. *FEBS Lett* 2003;**552**:28–34.
45. Jean Beltran PM, Cook KC, Cristea IM. Exploring and exploiting proteome organization during viral infection. *J Virol* 2017;**91**:e00268–17.
46. Baik SH, Jeong HS, Kim SJ, Yoon YK, Sohn JW, Kim MJ. A case of influenza associated fulminant myocarditis successfully treated with intravenous peramivir. *Infect Chemother* 2015;**47**:272–277.
47. Cobas M, Abbo L, Santos M, Baccini-Jauregui C, Pham S. Successful management of fulminant influenza A subtype H1N1 myocarditis. *BMJ Case Rep* 2010;**17**:2010:bcr0220102763.
48. Esfandiarei M, McManus BM. Molecular biology and pathogenesis of viral myocarditis. *Annu Rev Pathol Mech Dis* 2008;**3**:127–155.

Translational perspective

Influenza A virus (IAV) can infect several cell types in the mouse heart. Human IAV with the highest pathogenicity replicate more rapidly in mouse cardiomyocyte cultures and induce a cardiac pro-inflammatory state, which correlates with underlying molecular changes and mitochondrial dysfunction in human-induced pluripotent stem cell-derived cardiomyocytes. The data demonstrate that heart infection and associated damage need not be a consequence of lung pathology. In fact, direct cardiac pathogenicity with the virus reaching and infecting the heart seems more relevant, which supports the relevance of early detection of IAV in clinical cases with acute cardiac disease during influenza outbreaks.